ACCOUNTS
of chemical research

# Strategies for Increasing the Efficiency of Heterojunction Organic Solar Cells: Material Selection and Device Architecture

PAUL HEREMANS,* DAVID CHEYNS, AND BARRY P. RAND
*IMEC v.z.w., Kapeldreef 75, B-3001 Leuven, Belgium*

RECEIVED ON MARCH 18, 2009



## CONSPECTUS

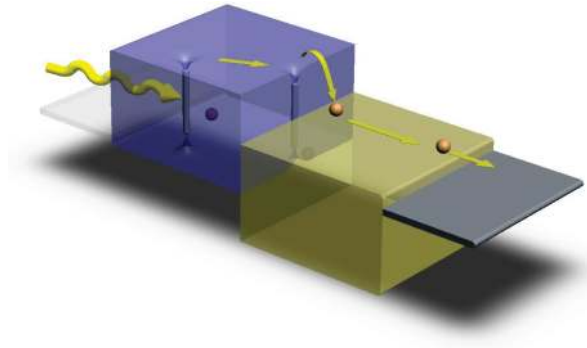

Thin-film blends or bilayers of donor- and acceptor-type organic semiconductors form the core of heterojunction organic photovoltaic cells. Researchers measure the quality of photovoltaic cells based on their power conversion efficiency, the ratio of the electrical power that can be generated versus the power of incident solar radiation. The efficiency of organic solar cells has increased steadily in the last decade, currently reaching up to 6%. Understanding and combating the various loss mechanisms that occur in processes from optical excitation to charge collection should lead to efficiencies on the order of 10% in the near future.

In organic heterojunction solar cells, the generation of photocurrent is a cascade of four steps: generation of excitons (electrically neutral bound electron−hole pairs) by photon absorption, diffusion of excitons to the heterojunction, dissociation of the excitons into free charge carriers, and transport of these carriers to the contacts. In this Account, we review our recent contributions to the understanding of the mechanisms that govern these steps. Starting from archetype donor−acceptor systems of planar small-molecule heterojunctions and solution-processed bulk heterojunctions, we outline our search for alternative materials and device architectures.

We show that non-planar phthalocynanines have appealing absorption characteristics but also have reduced charge carrier transport. As a result, the donor layer needs to be ultrathin, and all layers of the device have to be tuned to account for optical interference effects. Using these optimization techniques, we illustrate cells with 3.1% efficiency for the non-planar chloroboron subphthalocyanine donor. Molecules offering a better compromise between absorption and carrier mobility should allow for further improvements. We also propose a method for increasing the exciton diffusion length by converting singlet excitons into long-lived triplets. By doping a polymer with a phosphorescent molecule, we demonstrate an increase in the exciton diffusion length of a polymer from 4 to 9 nm. If researchers can identify suitable phosphorescent dopants, this method could be employed with other materials.

The carrier transport from the junction to the contacts is markedly different for a bulk heterojunction cell than for planar junction cells. Unlike for bulk heterojunction cells, the open-circuit voltage of planar-junction cells is independent of the contact work functions, as a consequence of the balance of drift and diffusion currents in these systems.

This understanding helps to guide the development of new materials (particularly donor materials) that can further boost the efficiency of single-junction cells to 10%. With multijunction architectures, we expect that efficiencies of 12−16% could be attained, at which point organic photovoltaic cells could become an important renewable energy source.

## Introduction

In 1986, Tang demonstrated an organic solar cell[1] with power conversion efficiency ($\eta_P$) equal to 1%, 1−2 orders of magnitude larger than that of other organic-based devices at that time. The key innovation was the introduction of an interface between two organic semiconductors, called the donor and the acceptor. Because excited states in

 

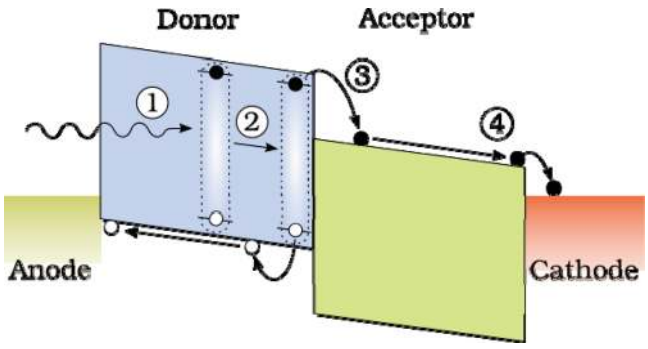


**FIGURE 1.** Energy diagram of an organic solar cell with a donor−acceptor interface. The four subsequent processes to generate photocurrent are (1) absorption of an incident photon to create an exciton, (2) diffusion of an exciton toward the donor−acceptor interface, (3) charge transfer of an exciton into an electron in the acceptor and hole in the donor, and (4) collection of charges at the contacts.



organic molecules, or excitons, are characterized by large binding energies, typically on the order of 0.2−1 eV, this donor−acceptor (DA) interface proved essential to efficiently dissociate excitons into free electrons and holes, which are then transported on the acceptor and donor materials, respectively, producing a photocurrent. This initial demonstration spurred a rapidly expanding research effort, which has produced cells with $\eta_P \approx 5-6\%$[2−4] and as high as 6.7%,[5] with 10% expected in the near future.[6−8] Efficiency gains have come mainly from improvements in molecular design and control of molecular ordering in the films.

Various material classes, including polymers and small molecules, are commonly used as either donor or acceptor.[8−11] In this Account, we focus on all-organic small-molecule-based and polymer/fullerene cells. The Account is structured by considering the various steps in the conversion of light into electrical current for organic solar cells with DA interfaces, from the absorption of light to the collection of carriers at the contacts. Within each process, we highlight the role that new materials and device architectures have played and will play in improving efficiency.

## From Photons to Photocurrent

In organic solar cells, a sequence of four steps converts incident solar illumination to photocurrent, These steps are outlined in Figure 1, where we show the energy diagram of an organic solar cell with a DA interface. The donor material has a smaller (with respect to the vacuum level) HOMO (highest occupied molecular orbital) and LUMO (lowest unoccupied molecular orbital) compared with the acceptor. As such, the donor is the hole transporting material and ideally makes ohmic contact with the anode, whereas the acceptor material transports electrons and contacts the cathode.

The first process shown in Figure 1 is that of absorption, the outcome of which is an exciton, which is able to diffuse within the layer in which it was created. The absorption efficiency ($\eta_A$) is largely controlled by the absorption spectra of the organic molecular layers, as well as their thickness, but also by the device architecture, as will be explained below. The second process is that of exciton diffusion, and the efficiency ($\eta_{ED}$) of this process is determined mainly by the exciton diffusion length ($L_D$), as well as the morphology of the DA interface. The process of exciton dissociation into free charges is characterized by an efficiency ($\eta_{CT}$, step 3) that is significant if energetically favorable. The percentage of dissociated excitons that are collected at the electrodes is the final process, termed the charge collection efficiency ($\eta_{CC}$). This process is sensitive mainly to the morphology and mobility of the active layers. Then, the overall efficiency of converting incident photons to current, or the external quantum efficiency ($\eta_{EQE}$), can be calculated via $\eta_{EQE}(\lambda, V) = \eta_A(\lambda)\eta_{ED}\eta_{CT}(V)\eta_{CC}(V)$. Here, $\lambda$ is the wavelength of incident light, and $V$ is the voltage across the cell.

The molecular structures of some of the materials discussed in this Account are shown in Figure 2. Of these, $C_{60}$, 1-(3-methoxycarbonyl)-propyl-1-phenyl-[6,6]-methanofullerene (PCBM), and *N*,*N*′-ditridecylperylene-3,4,9,10-tetracarboxylic diimide (PTCDI-$C_{13}H_{27}$) are acceptor molecules, while poly-3-hexylthiophene (P3HT), chloroboron subphthalocyanine (SubPc), chloroboron subnaphthalocyanine (SubNc), copper phthalocyanine (CuPc), and poly[2-methoxy-5-(3′,7′-dimethyloctyloxy)-1,4-phenylene vinylene] (MDMO-PPV) are donor molecules. Also, P3HT, MDMO-PPV, and PCBM are solution processed, while the others are deposited in vacuum from the vapor phase. There are two categories of device architecture that we discuss in this Account, namely, the planar heterojunction (HJ) and the bulk HJ (BHJ). In the latter, the two materials form an interpenetrating DA interface with a much larger surface area than that of the planar HJ. In the sections that follow, we discuss our recent progress in material selection and device architectures toward improvements in each of the four processes that contribute to $\eta_{EQE}$.

## Absorption

The strength and width of the absorption spectrum of a photoactive layer determines to a large extent its potential for harvesting incident solar radiation. Unlike crystalline inorganic semiconductors that absorb a continuous spectrum of photons with energy greater than their bandgap, organic semiconductors have well-defined electronic transitions that are typically quite narrow. Furthermore, these optical transitions tend to be very sensitive to their surroundings. For example,

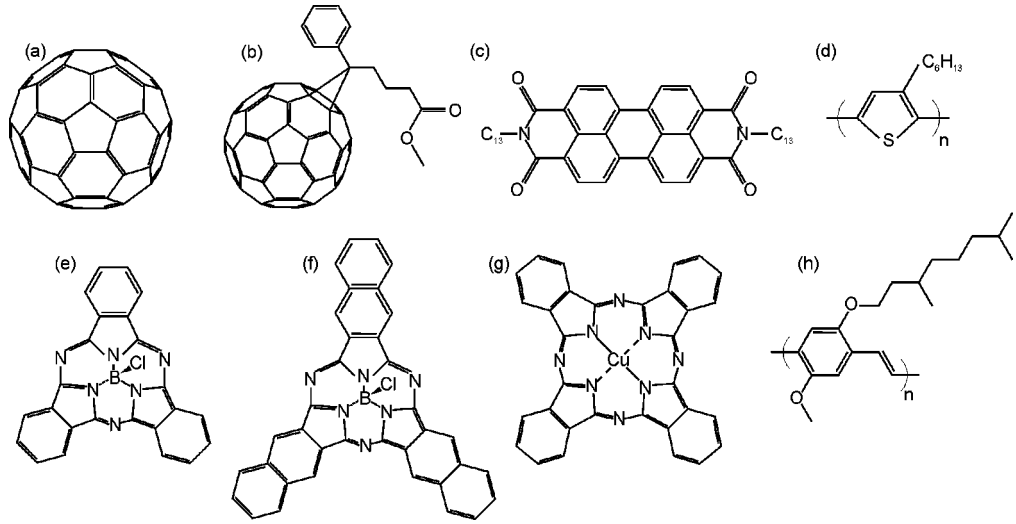


**FIGURE 2.** Molecular structures of some materials discussed in this Account: (a) $C_{60}$, (b) PCBM, and (c) PTCDI-$C_{13}H_{27}$ are acceptors, whereas (d) P3HT, (e) SubPc, (f) SubNc, (g) CuPc, and (h) MDMO-PPV are donors.

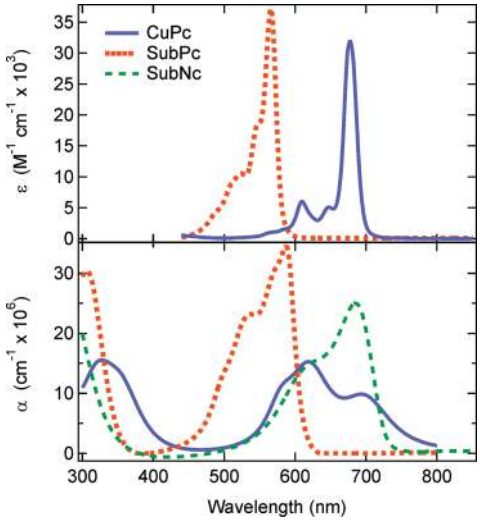


**FIGURE 3.** Molar absorptivities, $\varepsilon$, of CuPc and SubPc solutions (top) and absorption coefficients, $\alpha$, of CuPc, SubPc, and SubNc thin films (bottom). For solution spectra, CuPc is in 1-methylnapthalene ($8 \times 10^{-5}$ M) and SubPc is in toluene ($2.3 \times 10^{-5}$ M).

monomer absorption can be probed for molecules in the gas phase or in a very dilute solution, and in this case the probability of photon−molecule interaction is determined by the density of molecules and their oscillator strength. Upon transition to the solid state, intermolecular interactions are introduced. These interactions, which are determined by the crystal structure of the molecules and the tendency of a given molecule to aggregate, can have significant impact on their absorption spectrum.

As an example, we show in Figure 3 the solution and thin-film absorption spectra of CuPc and SubPc, two molecules that have found use in organic solar cells.[1,9,12−14] The molar absorptivity ($\varepsilon$) spectra of the Q-bands of CuPc and SubPc in solution show remarkably similar features, related to the different vibronic transitions of the first exciton absorption.[15] Moreover, the absorption strengths have comparable amplitudes, with peaks up to $\varepsilon = 3 \times 10^4$ $M^{-1}$ $cm^{-1}$. These spectra, recorded for very dilute solutions, can be considered as the monomeric absorption of these molecules. The absorption spectra of these same materials in the solid state, however, are quite dissimilar. In films as well as in poor solvents, planar phthalocyanines such as CuPc form aggregates and ultimately crystallize, as evidenced by the changes and broadening of the Q-band absorption. The strongest peak within the Q-band of the CuPc film is not the low-energy peak at $\lambda =$ 690 nm, which is the contribution from the CuPc monomer, but the peak at $\lambda = 620$ nm, associated with dimer absorption and indicative of the formation of cofacial aggregates of planar phthalocyanine molecules.[16,17] In contrast, the spectrum of a thin film of SubPc resembles very closely that of SubPc in solution. Here, each of the peaks within the Q-band of SubPc is preserved in transferring from solution to the solid state, albeit with a red shift of approximately 20 nm and changes in the relative strengths of each transition. This resemblance of the two spectra indicates weak intermolecular interactions between nonplanar SubPc molecules in the film. Another noteworthy point is that the peak absorption coefficient, $\alpha$, of the nonplanar SubPc and SubNc is considerably higher than that of CuPc. In fact, this trend is not completely uncommon, since other nonplanar phthalocyanines[18−20] are also known to absorb strongly.

Morphological and electrical characteristics of films of CuPc and SubPc corroborate the interpretation of the absorption spectra. Films of CuPc are polycrystalline, with relatively rough surface morphology and hole mobility on the order of $10^{-3}$

to $10^{-4}$ cm$^2$/(V s).[21] For SubPc, film formation is very smooth and amorphous[13] and mobility is considerably lower, on the order of $10^{-5}$ cm$^2$/(V s). The amorphous structure and low hole mobility are consistent with the minimal changes to the absorption spectra between solution and film.

The wider absorption window of crystalline films compared with amorphous films leads to the conclusion that the former are excellent candidates for bulk heterojunction single-junction cells. Ideally, the absorption spectrum of such materials should extend to ~750−850 nm. In addition, the higher charge carrier mobility expected for more crystalline films allows cells to be thicker, which will be more forgiving for large area devices. An example of a material where optimum performance correlates with crystallinity and relatively thick layers (200−300 nm) is the bulk heterojunction P3HT/fullerene blends. It should be noted, however, that multijunction cells may be better served with more amorphous materials that allow very smooth films that absorb strongly over a limited spectral window.

## Exciton Diffusion

The fraction of excitons that reach the DA interface is determined by the exciton diffusion length ($L_D$) and the location at which an exciton is created with respect to the nearest dissociation center. In this section, we will highlight the roles that device design and material selection play in the optimization of $\eta_{ED}$.

The fact that organic semiconductors possess large $\alpha$ as well as low mobility puts significant constraints on the thickness of layers used in organic solar cells. For example, layers that are thicker than 200−300 nm do not absorb significantly more light than a thinner film but exhibit a large series resistance. Therefore, optimal film thicknesses are less than the wavelength of incident light, producing optical interference effects. Reflection and transmission at each material interface creates a standing wave pattern, which depends on the complex indices of refraction and thicknesses of the layers within the structure. The transfer matrix method (TMM) can be used to accurately calculate this optical interference pattern at any incident wavelength and angle, and this corresponds directly to the exciton generation rate throughout the layer structure.[14,22,23] The percentage of excitons that reach a dissociation center is then calculated from the steady-state exciton generation profile by solving the diffusion equation, with $L_D$ as the critical parameter. Maximizing the photocurrent is then possible for planar and BHJ cells by tuning the thicknesses of the different layers to optimize the maxima and minima of the optical field in the device. We have successfully applied this optimization procedure to planar solar cells based on CuPc/$C_{60}$, SubPc/$C_{60}$, and SubNc/$C_{60}$ HJs, and the current density vs voltage characteristics for these devices are shown in Figure 4. They have $\eta_P$ equal to 1.6%, 3.1%, and 2.5%, respectively. In performing the optical calculations, $L_D$ was estimated by using the optical constants and fitting to the $\eta_{EQE}$ spectra (data not shown). Following this treatment, we obtain $L_D \approx 9$ nm for both SubPc[13] and SubNc,[24] while $L_D \approx 10$ nm for CuPc.[14] Despite its less desirable spectrum compared with CuPc (cf. Figure 3), the current of optimized SubPc cells can be made comparable to that of CuPc cells; SubNc has a larger short-circuit current, ($J_{SC}$), but its overall efficiency is limited by a poor fill factor (FF) resulting from its low mobility.

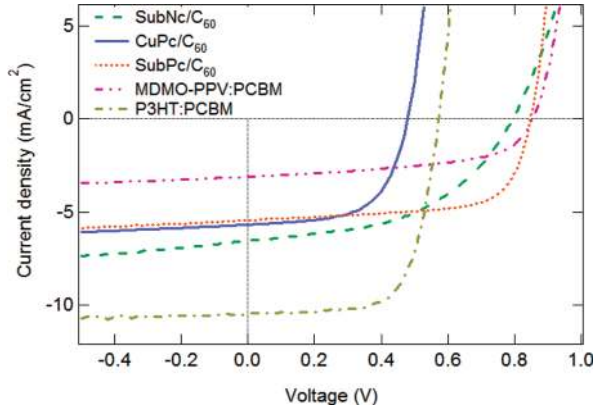


**FIGURE 4.** Current density vs voltage characteristics of various planar and bulk heterojunction devices under 1 sun (100 mW/cm$^2$) AM1.5D illumination.

As a guideline to obtain longer diffusion lengths for singlet excitons, we remind that singlets migrate by a sequence of Förster transfer processes. Therefore, for a long $L_D$, the material in solid film should possess a long exciton lifetime and strong optical transitions (emission as well as absorption), and the spectral overlap between emission and absorption should be large, implying a small Stokes shift. Good molecular ordering is favorable because it reduces the energetic disorder, thereby reducing the Stokes shift in films.[25] In some materials, generated singlet excitons rapidly transfer to triplets. One example of such a molecule is $C_{60}$, which has a near-unity intersystem crossing (ISC) yield of singlet to triplet excitons.[26] Triplets migrate by Dexter transfer, characterized by a smaller diffusion coefficient than singlets. However, the orders-of-magnitude longer triplet lifetime results in long triplet diffusion lengths, for example, $L_D \approx 40$ nm for the case of $C_{60}$.[14] This raises the question whether triplets could also be employed in donor materials as exciton vehicles with increased $L_D$.

Triplets are not generated directly by optical excitation of fluorescent hosts. We recently explored the use of a process

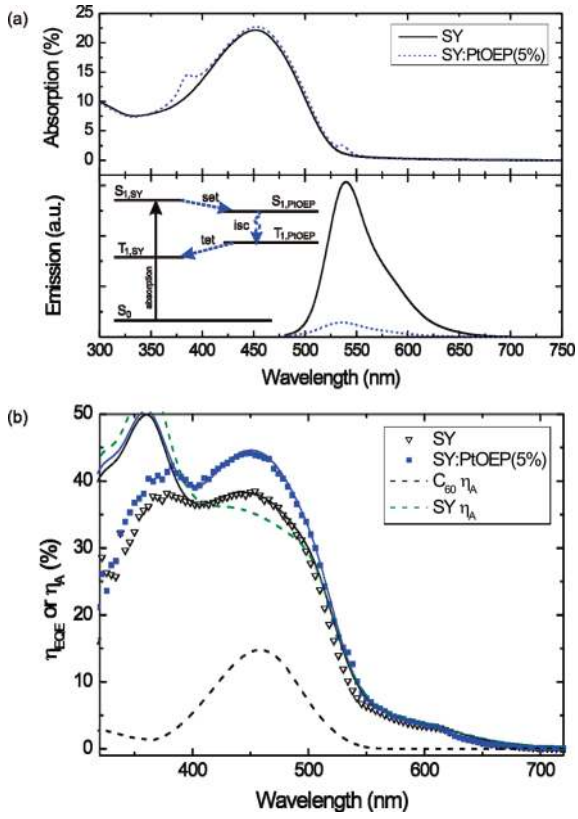


**FIGURE 5.** (a) Absorption (top) and emission (bottom) of 15 nm thick SY and SY:PtOEP(5%) films. The inset shows the sensitized phosphorescence scheme for SY:PtOEP. Following photon absorption in SY to excite a molecule from the ground state ($S_0$) to the first excited singlet state ($S_{1,SY}$) there is singlet energy transfer (set) to $S_{1,PtOEP}$. Intersystem crossing (isc) then converts $S_{1,PtOEP}$ to triplet excitons on $T_{1,PtOEP}$. Finally, the lower energy $T_{1,SY}$ quenches the PtOEP triplets. (b) Measured external quantum efficiency ($\eta_{EQE}$) spectra for planar device structures with 15 nm thick donor layers of pure SY (open black triangles) or SY:PtOEP(5%) (filled blue squares) and 30 nm thick acceptor layers of $C_{60}$. The solid lines show the calculated $\eta_{EQE}$ spectra, with colors corresponding to the data points. The dashed lines show calculated absorption efficiencies ($\eta_A$) of the SY (black) and $C_{60}$ (green) layers.

known as sensitized phosphorescence to efficiently convert singlets into triplets in conventional fluorescent donor materials.[27] A small percentage of a phosphorescent dopant can efficiently capture initially generated singlet excitons on the host and transform them into triplets, after which they cascade further into the triplet level of the host. In this way, the fluorescent host material is still used for light absorption as well as for charge and exciton transport. We demonstrate this effect in the phenyl-substituted PPV polymer Super Yellow (SY), doped with the phosphorescent molecule platinum octaethylporphyrin (PtOEP). The absorption and emission of the neat SY film, as well as of films doped with 5% of PtOEP, are shown in Figure 5a. The absorption features of PtOEP are present, though weak, in the doped films at $\lambda = 385$ and 535 nm. The SY emission at $\lambda = 540$ nm is strongly quenched as a result of the introduction of the dopant, suggesting the pathway shown schematically in the inset to Figure 5a, where SY singlets efficiently transfer to triplets on the guest. Furthermore, PtOEP phosphorescence at $\lambda = 650$ nm is not present, because the PtOEP triplet is rapidly quenched to the lower triplet state of SY (1.6 eV for SY compared with 1.9 eV for PtOEP).[28]

As evidence of this mechanism in a device, we plot the $\eta_{EQE}$ spectra of doped and undoped devices consisting of a SY/$C_{60}$ DA interface in Figure 5b, along with the TMM-calculated $\eta_A$ spectra of SY and $C_{60}$. The SY contribution is centered at $\lambda = 455$ nm, whereas $C_{60}$ produces the shoulder at $\lambda = 435$ nm and the tail extending to $\lambda = 650$ nm. The $\eta_{EQE}$ spectrum of the device with a pure SY donor layer shows features of both SY and $C_{60}$, and the best fit yields $L_D \approx 4$ nm. The $\eta_{EQE}$ spectrum of the SY:PtOEP(5%) device, however, shows an enhancement of the SY signal of ~40% compared with the undoped SY device. In this case, $L_D$ increases to 9 nm due to the longer lifetime of SY triplet excitons, and correspondingly $\eta_{ED}$ also increases.

Instead of developing techniques to increase $L_D$ as described above, the most-explored approach to-date is to reduce the average distance between DA interfaces by forming a BHJ. This approach has been successfully applied to solar cells produced by both solution processing and thermal evaporation, with $\eta_{ED}$ approaching unity. We will not go into further detail about this device architecture, because this topic has been the subject of numerous reviews.[8−11] The major disadvantages of the BHJ approach stem from the lack of direct morphological control and the fact that the nanoscale morphology is not thermodynamically stable. Furthermore, very fine BHJ morphologies may cause nongeminate bulk recombination of charge carriers. Therefore, as a general guideline, donors with larger exciton diffusion lengths will allow coarser BHJ morphologies and are preferred. The ideal BHJ is probably one that mimics an interdigitated structure composed of distinct donor and acceptor lamellae, as can be achieved by nanoimprint technology.[29]

## Charge Transfer and Charge Collection

An exciton reaching a DA interface dissociates into a so-called geminate pair, a Coulombically bound electron and hole. This charge pair still experiences an appreciable binding energy (up to 0.5 eV), and a subsequent dissociation step is required to obtain free charge carriers from initial excitons, with a global efficiency $\eta_{CT}$. In fact, the nature of the geminate pair state and the conditions for efficient charge transfer are a matter of con-

tinuing research.[30,31] Because it is difficult to determine the point at which the geminate pair is fully dissociated, we also consider the last step in the photoconversion process, that of $\eta_{CC}$, together in the same section. Whereas $\eta_A$ and $\eta_{ED}$ influence only $J_{SC}$, $\eta_{CT}$ and $\eta_{CC}$ also have important consequences to the open-circuit voltage ($V_{OC}$) and FF.[7,32,33] The limiting value of $V_{OC}$ for a DA pair that still allows complete exciton dissociation into free carriers is given by the difference between HOMO of the donor ($HOMO_D$) and LUMO of the acceptor ($LUMO_A$) minus at least the binding energy of the geminate pair at the DA interface.[7] Estimations for that latter term range from 0.3 to 0.8 eV, and this uncertainty is to a large extent responsible for the large variety of estimations of the ultimate efficiency of single-junction organic cells, ranging from 8% to 15%.[6−8,11] Furthermore, for identical material systems, there are differences in $V_{OC}$ between planar HJ and BHJ devices, as a result of the distribution of exciton dissociation centers in the layer structure.

In the case of a planar HJ, charges are only generated at a single DA interface within the device structure. Consequently, large gradients in carrier concentrations are present between the DA interface and the collecting contacts, producing appreciable diffusion currents, in addition to drift currents.[34,35] Since transport occurs through pure acceptor or donor layers, it can be assumed that no charges of the opposite sign are present, and thus recombination within the bulk is unlikely. Thus, $\eta_{CC}$ is determined by the carrier mobility as well as the charge distribution within that layer.[32] Remarkably, the balance between drift and diffusion currents at $V_{OC}$ means that $V_{OC}$ is independent of the contact metal work function ($\phi$), instead being determined by $HOMO_D - LUMO_A$ and by the concentrations of free carriers at the DA interface. Schematic band diagrams at $V_{OC}$ for low and high injection barriers at the contacts ($\Delta\phi$) are shown in Figure 6a and b, respectively. In both cases, the photogenerated carrier density at the DA interface and the HOMO and LUMO levels are equal. The balance of drift and diffusion currents produces equal $V_{OC}$. Nevertheless, the steady-state carrier density is lower in the case of high $\Delta\phi$, and this will cause both higher series resistance and lower FF.

In a BHJ, the photogenerated carrier profile is distributed throughout the layer. In most operation regimes, diffusion currents in the blend are insignificant compared with drift by the internal field, assumed here to be homogeneous in the bulk. The $V_{OC}$ for BHJs therefore depends on the built-in field, which in turn is determined by $\phi$ of anode and cathode.[36] The resulting band diagrams[37] (Figure 6c,d) are substantially different from the ones for planar HJs. The first case (Figure 6c), with small $\Delta\phi$ or a high built-in field, leads to a maximum $V_{OC}$ that

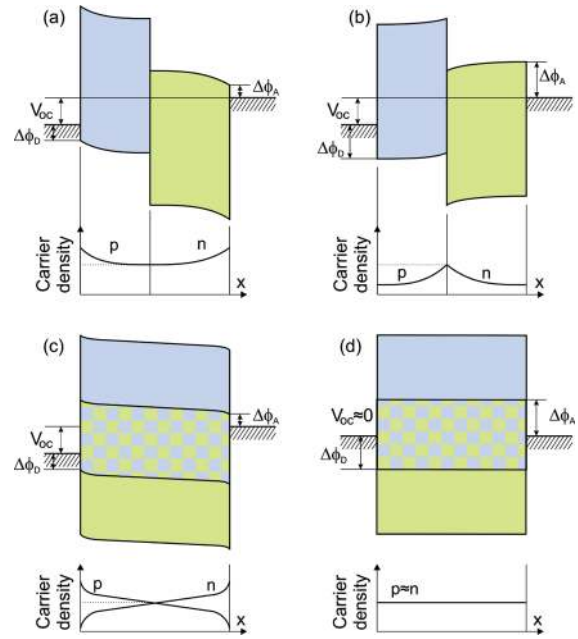


**FIGURE 6.** Schematic band diagrams and hole (p) and electron (n) carrier densities at open-circuit voltage ($V_{OC}$) conditions vs position ($x$) within the device for (a, b) planar heterojunctions and (c, d) bulk heterojunctions. The carrier injection barriers ($\Delta\phi$) at the contacts are either (a, c) small or (b, d) large.

is close to $HOMO_D - LUMO_A$. For high $\Delta\phi$ (Figure 6d), however, the built-in field is very low and limits the maximum $V_{OC}$.

Another challenge for the BHJ cell is achieving a high $\eta_{CC}$. Hole and electron transport occurs, respectively, via the separate donor and acceptor molecular networks, but due to the abundance of nearby DA interfaces, carrier recombination processes are possible. A delicate optimization of the phase separation is needed to provide direct transport paths for the carriers to the contacts. Unless $L_D$ can be made sufficiently large, a trade-off exists between finely distributed DA interfaces for high $\eta_{ED}$ versus coarser phase separation for high $\eta_{CC}$. In Figure 4, we provide examples of optimized blends of MDMO-PPV/PCBM and P3HT/PCBM, which show simultaneously high $J_{SC}$ and FF and $\eta_P$ of 1.5% and 4.1%, respectively. For small molecule BHJs, there is a tendency to form uniformly mixed blends without significant phase separation, leading to devices with low mobilities, low $\eta_{CC}$, and high series resistance.[21] Some methods to successfully combat this problem are currently being investigated, such as thermal annealing[38] or alternate deposition of ultrathin donor and acceptor layers.[39,40] Finally, as a material guideline for donor/fullerene cells, we deduce that the hole mobility in the donor should be at least as large as the electron mobility in the fullerene, that is, on the order of $10^{-2}$ $cm^2/(V\ s)$, so as not to be the limiting factor in charge transport and fill factor.

## Conclusion

The complexity of the heterojunction organic solar cell stems from the delicate balance that exists between the different material properties and from the fact that many paths may be followed corresponding to different optimization strategies. To maximize the efficiency of donor/fullerene systems, particularly for single-junction architectures, it is clear that favorable donor properties are strong optical absorption over a broad wavelength range extending to 750−850 nm, high hole mobility of $10^{-2}$ $cm^2/(V\ s)$, and long $L_D$. These properties allow coarse BHJ cells with appreciable and manufacturable thicknesses. For multijunction cells, thin and smooth films absorbing over a limited spectral window are preferred. We showed that the relatively small $L_D$ typical of singlet excitons can be strongly increased by adding small quantities of well-chosen phosphorescent dopants. Finally, we conclude that the attainable $V_{OC}$ remains a large unknown in the ultimate efficiency of organic solar cells, because no comprehensive model currently exists that can predict the difference between the $V_{OC}$ and $HOMO_D - LUMO_A$. In contrast, an understanding is being acquired for the role of the work function of the contact metals on $V_{OC}$ in planar and bulk heterojunction cells. Today's best BHJ cells are optimized in terms of $\eta_{ED}$ and $\eta_{CT}$. The other steps in the conversion of photons to photocurrent still can be improved, and it is clear that new materials have a key role to play in that process.



### BIOGRAPHICAL INFORMATION

**Paul Heremans** received M.S. and Ph.D. degrees in electrical engineering from the Katholieke Universiteit Leuven, Belgium, in 1984 and 1990, respectively. During part of that time, he also worked at the IBM T.J. Watson Research Center. His main research focus today is organic and oxide thin-film electronics, including backplanes for OLED displays, RFID tags, sensors, and memories, as well as organic photovoltaics. He is currently an IMEC research fellow and professor of Electrical Engineering at the Katholieke Universiteit Leuven.

**David Cheyns** received M.S. and Ph.D. degrees in electrical engineering from the Katholieke Universiteit Leuven, Belgium, in 2003 and 2008, respectively, while doing research on planar heterojunction organic solar cells in the Polymer and Molecular Electronics group at IMEC in Leuven, Belgium. Presently he is working on organic solar cells as a senior scientist within the same research group.

**Barry P. Rand** earned a B.E. in electrical engineering from The Cooper Union in 2001. He then received M.A. and Ph.D. degrees in electrical engineering from Princeton University in 2003 and 2007, respectively. His Ph.D. thesis was on the physics and optimization of organic solar cells. Since 2007, he has been a senior scientist in the Polymer and Molecular Electronics group at IMEC in Leuven, Belgium, working on the optimization and manufacturability of organic-based solar cells.

### FOOTNOTES

*AUTHOR EMAIL ADDRESS: Paul.Heremans@imec.be. Also at ESAT, Katholieke Universiteit Leuven, B-3001 Leuven, Belgium.

### REFERENCES

1 Tang, C. W. 2-Layer organic photovoltaic cell. *Appl. Phys. Lett.* **1986**, *48*, 183–185.
2 Li, G.; Shrotriya, V.; Huang, J. S.; Yao, Y.; Moriarty, T.; Emery, K.; Yang, Y. High-efficiency solution processable polymer photovoltaic cells by self-organization of polymer blends. *Nat. Mater.* **2005**, *4*, 864–868.
3 Xue, J.; Rand, B. P.; Uchida, S.; Forrest, S. R. A hybrid planar-mixed molecular heterojunction photovoltaic cell. *Adv. Mater.* **2005**, *17*, 66–70.
4 Park, S. H.; Roy, A.; Beaupré, S.; Cho, S.; Coates, N.; Moon, J. S.; Moses, D.; Leclerc, M.; Lee, K.; Heeger, A. J. Bulk heterojunction solar cells with internal quantum efficiency approaching 100%. *Nat. Photonics* **2009**, *3*, 297–302.
5 Kim, J. Y.; Lee, K.; Coates, N. E.; Moses, D.; Nguyen, T.; Dante, M.; Heeger, A. J. Efficient tandem polymer solar cells fabricated by all-solution processing. *Science* **2007**, *317*, 222–225.
6 Koster, L. J. A.; Mihailetchi, V. D.; Blom, P. W. M. Ultimate efficiency of polymer/fullerene bulk heterojunction solar cells. *Appl. Phys. Lett.* **2006**, *88*, 093511.
7 Rand, B. P.; Burk, D. P.; Forrest, S. R. Offset energies at organic semiconductor heterojunctions and their influence on the open-circuit voltage of thin-film solar cells. *Phys. Rev. B,* **2007**, *75*, 115327.
8 Riede, M.; Mueller, T.; Tress, W.; Schueppel, R.; Leo, K. Small-molecule solar cells - status and perspectives. *Nanotechnology* **2008**, *19*, 424001.
9 Rand, B. P.; Genoe, J.; Heremans, P.; Poortmans, J. Solar cells utilizing small molecular weight organic semiconductors. *Prog. Photovoltaics* **2007**, *15*, 659–676.
10 Thompson, B. C.; Fréchet, J. M. J. Polymer-fullerene composite solar cells. *Angew. Chem., Int. Ed.* **2008**, *47*, 58–77.
11 Dennler, G.; Scharber, M.; Brabec, C. J. Polymer-fullerene bulk-heterojunction solar cells. *Adv. Mater.* **2009**, *21*, 1323–1338.
12 Mutolo, K. L.; Mayo, E. I.; Rand, B. P.; Forrest, S. R.; Thompson, M. E. Enhanced open-circuit voltage in subphthalocyanine/C-60 organic photovoltaic cells. *J. Am. Chem. Soc.* **2006**, *128*, 8108–8109.
13 Gommans, H.; Cheyns, D.; Aernouts, T.; Girotto, C.; Poortmans, J.; Heremans, P. Electro-optical study of subphthalocyanine in a bilayer organic solar cell. *Adv. Funct. Mater.* **2007**, *17*, 2653–2658.
14 Peumans, P.; Yakimov, A.; Forrest, S. R. Small molecular weight organic thin-film photodetectors and solar cells. *J. Appl. Phys.* **2003**, *93*, 3693–3723.
15 Claessens, C. G.; Gonzalez-Rodriguez, D.; Torres, T. Subphthalocyanines: Singular nonplanar aromatic compounds - synthesis, reactivity, and physical properties. *Chem. Rev.* **2002**, *102*, 835–853.
16 Ogata, H.; Higashi, R.; Kobayashi, N. Electronic absorption spectra of substituted phthalocyanines in solution and as films. *J. Porphyrins Phthalocyanines* **2003**, *7*, 551–557.
17 George, R. D.; Snow, A. W.; Shirk, J. S.; Barger, W. R. The alpha substitution effect on phthalocyanine aggregation. *J. Porphyrins Phthalocyanines* **1998**, *2*, 1–7.
18 Bailey-Salzman, R. F.; Rand, B. P.; Forrest, S. R. Near-infrared sensitive small molecule organic photovoltaic cells based on chloroaluminum phthalocyanine. *Appl. Phys. Lett.* **2007**, *91*, 013508.
19 Brumbach, M.; Placencia, D.; Armstrong, N. R. Titanyl phthalocyanine/$C_{60}$ heterojunctions: Band-edge offsets and photovoltaic device performance. *J. Phys. Chem. C* **2008**, *112*, 3142–3151.
20 Rand, B. P.; Xue, J.; Yang, F.; Forrest, S. R. Organic solar cells with sensitivity extending into the near infrared. *Appl. Phys. Lett.* **2005**, *87*, 233508.
21 Rand, B. P.; Xue, J.; Uchida, S.; Forrest, S. R. Mixed donor-acceptor molecular heterojunctions for photovoltaic applications. I. Material properties. *J. Appl. Phys.* **2005**, *98*, 124902.
22 Pettersson, L. A. A.; Roman, L. S.; Inganäs, O. Modeling photocurrent action spectra of photovoltaic devices based on organic thin films. *J. Appl. Phys.* **1999**, *86*, 487–496.
23 Cheyns, D.; Rand, B. P.; Verreet, B.; Genoe, J.; Poortmans, J.; Heremans, P. The angular response of ultrathin film organic solar cells. *Appl. Phys. Lett.* **2008**, *92*, 243310.
24 Verreet, B.; Schols, S.; Cheyns, D.; Rand, B. P.; Gommans, H.; Aernouts, T.; Heremans, P.; Genoe, J. The characterization of chloroboron (III) subnaphthalocyanine thin films and their application as a donor material for organic solar cells. *J. Mater. Chem.* **2009**, *19*, 5295–5297.

25 Brunner, K.; Tortschanoff, A.; Warmuth, Ch.; Bässler, H.; Kauffmann, H. F. Site torsional motion and dispersive excitation hopping transfer in $\pi$-conjugated polymers. *J. Phys. Chem. B* **2000**, *104*, 3781–3790.

26 Terazima, M.; Hirota, N.; Shinohara, H.; Saito, Y. Photothermal investigation of the triplet state of $C_{60}$. *J. Phys. Chem.* **1991**, *95*, 9080–9085.

27 Rand, B. P.; Schols, S.; Cheyns, D.; Gommans, H.; Girotto, C.; Genoe, J.; Heremans, P.; Poortmans, J. Organic solar cells with sensitized phosphorescent absorbing layers. *Org. Electron.* **2009**, *10*, 1015–1019.

28 Laquai, F.; Im, C.; Kadashchuk, A.; Bässler, H. Sensitized intrinsic phosphorescence from a poly(phenylene-vinylene) derivative. *Chem. Phys. Lett.* **2003**, *375*, 286–291.

29 Cheyns, D.; Vasseur, K.; Rolin, C.; Genoe, J.; Poortmans, J.; Heremans, P. Nanoimprinted semiconducting polymer films with 50 nm features and their application to organic heterojunction solar cells. *Nanotechnology* **2008**, *19*, 424016.

30 Westenhoff, S.; Howard, I. A.; Hodgkiss, J. M.; Kirov, K. R.; Bronstein, H. A.; Williams, C. K.; Greenham, N. C.; Friend, R. H. Charge recombination in organic photovoltaic devices with high open-circuit voltages. *J. Am. Chem. Soc.* **2008**, *130*, 13653–13658.

31 Ohkita, H.; Cook, S.; Astuti, Y.; Duffy, W.; Tierney, S.; Zhang, W.; Heeney, M.; McCulloch, I.; Nelson, J.; Bradley, D. D. C.; Durrant, J. R. Charge carrier formation in polythiophene/fullerene blend films studied by transient absorption spectroscopy. *J. Am. Chem. Soc.* **2008**, *130*, 3030–3042.

32 Cheyns, D.; Poortmans, J.; Heremans, P.; Deibel, C.; Verlaak, S.; Rand, B. P.; Genoe, J. Analytical model for the open-circuit voltage and its associated resistance in organic planar heterojunction solar cells. *Phys. Rev. B,* **2008**, *77*, 165332.

33 Vandewal, K.; Gadisa, A.; Oosterbaan, W. D.; Bertho, S.; Banishoeib, F.; Severen, I. V.; Lutsen, L.; Cleij, T. J.; Vanderzande, D.; Manca, J. V. The relation between open-circuit voltage and the onset of photocurrent generation by charge-transfer absorption in polymer: fullerene bulk heterojunction solar cells. *Adv. Funct. Mater.* **2008**, *18*, 2064–2070.

34 Gregg, B. A.; Hanna, M. C. Comparing organic to inorganic photovoltaic cells: Theory, experiment, and simulation. *J. Appl. Phys.* **2003**, *93*, 3605–3614.

35 Barker, J. A.; Ramsdale, C. M.; Greenham, N. C. Modeling the current-voltage characteristics of bilayer polymer photovoltaic devices. *Phys. Rev. B* **2003**, *67*, 075205.

36 Mihailetchi, V. D.; Blom, P. W. M.; Hummelen, J. C.; Rispens, M. T. Cathode dependence of the open-circuit voltage of polymer-fullerene bulk heterojunction solar cells. *J. Appl. Phys.* **2003**, *94*, 6849–6854.

37 Koster, L. J. A.; Smits, E. C. P.; Mihailetchi, V. D.; Blom, P. W. M. Device model for the operation of polymer/fullerene bulk heterojunction solar cells. *Phys. Rev. B,* **2005**, *72*, 085205.

38 Peumans, P.; Uchida, S.; Forrest, S. R. Efficient bulk heterojunction photovoltaic cells using small-molecular-weight organic thin films. *Nature* **2003**, *425*, 158–162.

39 Yang, F.; Sun, K.; Forrest, S. R. Efficient solar cells using all-organic nanocrystalline networks. *Adv. Mater.* **2007**, *19*, 4166–4171.

40 Hong, Z. R.; Maennig, B.; Lessmann, R.; Pfeiffer, M.; Leo, K.; Simon, P. Improved efficiency of zinc phthalocyanine/$C_{60}$ based photovoltaic cells via nanoscale interface modification. *Appl. Phys. Lett.* **2007**, *90*, 203505.